

# A Single-Parameter Factor-Graph Image Prior

Tianyang Wang, Ender Konukoglu, Hans-Andrea Loeliger

Dept. of Information Technology and Electrical Engineering

ETH Zurich, Switzerland

tianwang@isi.ee.ethz.ch, ender.konukoglu@vision.ee.ethz.ch, loeliger@isi.ee.ethz.ch

**Abstract**—We propose a novel piecewise smooth image model with piecewise constant local parameters that are automatically adapted to each image. Technically, the model is formulated in terms of factor graphs with NUP (normal with unknown parameters) priors, and the pertinent computations amount to iterations of conjugate-gradient steps and Gaussian message passing. The proposed model and algorithms are demonstrated with applications to denoising and contrast enhancement.

**Index Terms**—factor graphs, image processing, NUP priors, scale factor estimation, iteratively reweighted least-squares

## I. INTRODUCTION

Modern methods for image processing are mostly based on deep neural networks. However, deep neural networks need to be trained on large data bases and are prone to complex hallucinations, which limits their attractivity in some applications. Moreover, adapting such methods to different distributions and imaging tasks usually requires the networks to be retrained.

By contrast, explicit prior models need no training, and their inductive bias is more transparent and justifiable. It is therefore desirable to improve the performance and flexibility of such models even in the era of deep learning.

One class of such models (or regularizers) simply penalizes the difference between neighboring pixels with a suitable cost function. The most popular such priors/regularizers are based on the L1 norm and favor piecewise constant images; this includes total-variation (TV) regularization [1], [2], total generalized variation (TGV) [3], and structure tensor total variation (STV) [4].

Another class of such models penalizes second-order differences [5]–[7]. However, the method of [7] requires three global parameters to be tuned.

Better results have been reported for penalizing pixel differences with cost functions that are convex for small pixel differences and concave for large pixel differences [8]; the convex part prefers smoothly varying areas while the concave part allows sharp edges. However, the prior proposed in [8] has two global parameters that need to be tuned and cannot easily be adapted to different parts of an image.

In this paper, we propose a novel image model that is more flexible, but also more complex, than such priors/regularizers in the prior literature. Like the model of [8], the proposed model favors piecewise smooth images, but unlike [8], the proposed model works with many local parameters. Despite this additional model complexity, these parameters are automatically adapted to each image. There is only one global

parameter, which is interpretable and determines the tradeoff between matching the data and fitting the model; it is the only parameter that must be set by the user.

Technically, the proposed model uses both NUP (normal with unknown parameters) priors [9] as well as a method proposed in [10] to estimate piecewise constant scale factors. With these ideas, the model fitting can be reduced to variations of iteratively reweighted least squares using both conjugate gradient steps and Gaussian message passing. The use of all these techniques in concert may be of interest beyond the specific model of this paper.

The viability of the proposed model and algorithms are demonstrated with applications to denoising and contrast enhancement, and with additional applications and examples in the appendix of the arXiv version (arXiv:2601.08749).

## II. PROPOSED MODEL AND ESTIMATION ALGORITHM

We will work with images consisting of pixels that are arranged in a rectangular grid. For ease of notation, we use only single indices for pixel values, e.g.,  $y_n \in \mathbb{R}$  for grayscale and  $y_n \in \mathbb{R}^3$  for color images.

In this paper, we assume a very simple observation model where a latent pixel value  $Y_n$  is related to an observed noisy pixel value  $\tilde{Y}_n = \tilde{y}_n$  by

$$\tilde{Y}_n = Y_n + Z_n, \quad (1)$$

where  $Z_n$  is white Gaussian noise with variance  $\sigma_Z^2$  for gray scale and with covariance matrix  $\sigma_Z^2 I \in \mathbb{R}^{3 \times 3}$  for color images. The assumed scalar noise variance  $\sigma_Z^2 > 0$  is the mentioned global parameter that determines the tradeoff between fitting the data and matching the model.

Experiments with, and variations of, this setting will be discussed in Section III. Using the proposed model with nontrivial observations models is certainly possible, but will not be considered in this paper.

The basic idea of the proposed model is to encourage the latent pixel values  $Y_n$  to be (approximately) piecewise smooth, with unsupervised partitioning and locally adapted parameters, as will be detailed in Sections II-A to II-C.

An augmentation of the model (described in Section II-D) aims at getting back some details (e.g., texture) into the smooth parts that might have been oversmoothed by the basic model.

### A. Basic Model

For every row and every column of the image, there is a state space model with latent state  $X_n$  (comprising the pixel

intensity and the slope) evolving along the row or column, respectively, according to

$$X_n = AX_{n-1} + BU_n + BSs_n \quad \text{and} \quad Y_n = CX_n \quad (2)$$

where  $n = 1, 2, \dots$ , indexes the pixels in the given row (or column), and

$$A = \begin{pmatrix} I & I \\ 0 & I \end{pmatrix}, \quad BU = \begin{pmatrix} I \\ 0 \end{pmatrix}, \quad BS = \begin{pmatrix} 0 \\ I \end{pmatrix}, \quad C = (I, 0), \quad (3)$$

where  $I$  is a  $3 \times 3$  identity matrix for color images and  $I = 1$  for grayscale images. Note that the latent pixel value  $Y_n$  is simply the upper part of  $X_n$ . Note also that, without an input (i.e., for  $U_n = S_n = 0$  for all  $n$ ), the pixel values  $Y_1, Y_2, \dots$  follow a straight line in the intensity space, with a slope defined by the (constant) lower part of  $X_n$ .

The inputs  $U_n$  and  $S_n$  in (2) will be referred to as level step inputs and slope noise inputs, respectively. The level step inputs  $U_n$  are intended to be sparse (as detailed below), with a nonzero value of  $U_n$  indicating an edge in the image. In smooth parts of the image,  $U_n$  is intended to be (approximately) zero, but the slope noise  $S_n$  can change the slope of the line model (2), as will be discussed in Section II-B.

The state space models for the different rows and columns are independent, but coupled by the condition that the latent pixel value  $Y_n$  in the pertinent row model equals its value in the pertinent column model, as illustrated in Fig. 1.

The inputs  $U_n$  are i.i.d. random with a sparsifying prior

$$p(u_n) \propto \exp(-\beta \|u_n\|^p) \quad (4)$$

with  $0 < p \leq 2$ . (A fixed value  $p \approx 0.3$  seems to work well.)

For computational tractability, we will use the well-known NUP representation of (4) as

$$\exp(-\beta \|u_n\|^p) = \max_{\sigma_{U_n}^2} g(\sigma_{U_n}) \exp\left(-\frac{\|u_n\|^2}{2\sigma_{U_n}^2}\right) \quad (5)$$

with a suitable function  $g$ . The maximizing  $\sigma_{U_n}^2$  in (5) is well-known [10], [11] to be

$$\sigma_{U_n}^2 = \frac{\|u_n\|^{2-p}}{\beta p} \quad (6)$$

### B. Slope Noise $S_n$ with Piecewise Constant Variance

The slope noise inputs  $S_n$  are independent zero-mean Gaussian with variance  $R_n^{-2}$  (or covariance matrix  $R_n^{-2}I$ ). The (scalar) parameters  $R_n$  are not fixed, but modeled as (approximately) piecewise constant. Specifically, we use the simple state space model

$$R_n = R_{n-1} + \Delta_n, \quad (7)$$

with i.i.d. random inputs  $\Delta_n$  with a sparsifying prior

$$p(\Delta_n) \propto \exp(-\beta_\Delta \|\Delta_n\|^p), \quad (8)$$

for which we use the same NUP representation as in (5), i.e.,

$$\sigma_{\Delta_n}^2 = \frac{\|\Delta_n\|^{2-p}}{p\beta_\Delta} \quad (9)$$

A factor graph of the entire basic model is shown in Fig. 1. For computational tractability, the dashed box in Fig. 1 uses the NUP representation

$$|r_n|^m \exp(-r_n^2 \|s_n\|^2/2) = \max_{\theta_n} h(r_n, \theta_n) \exp(-r_n^2 \|s_n\|^2/2) \quad (10)$$

proposed in [10] (with  $m = 1$  for grayscale and  $m = 3$  for color), with a suitable function  $h$  and parameters  $\theta_n$ . Using (10), [10] obtains a Gaussian message  $\tilde{\mu}_{R_n''}(r_n)$  with mean

$$\tilde{m}_{R''} = \beta_n \tilde{\sigma}_{R''}^2 \quad (11)$$

and variance

$$\tilde{\sigma}_{R''}^2 = (\|s_n\|^2 - \hat{r}_n^{-2} + \beta_n |\hat{r}_n|^{-1})^{-1}, \quad (12)$$

where  $\beta_n$  is a free parameter and  $\hat{r}_n$  is the previous value of  $R_n$  in the iterative estimation algorithm. In a recent improvement due to Lukaj [12], (11) and (12) are replaced by

$$\tilde{m}_{R''} = |\hat{r}_n|^{-1} \|s_n\|^{-2} \quad (13)$$

and variance

$$\tilde{\sigma}_{R''}^2 = \|s_n\|^{-2}, \quad (14)$$

respectively, which may formally be obtained by specializing (11) and (12) to  $\beta_n = |\hat{r}_n|^{-1}$ .

### C. Estimation Algorithm

The model is constructed such that, for fixed  $\sigma_{U_n}^2$  and  $R_n = r_n$  (for all  $n$  in all rows and all columns), the variables  $U_n, S_n, X_n, Y_n$  are jointly Gaussian, and computing the joint MAP estimates of these variables amounts to a sparse least squares problem (where rows and columns remain coupled). In our experience so far, the most attractive method to solve this least squares problem is the conjugate gradient algorithm.

Moreover, for fixed  $s_n$  (for all  $n$  in all rows and all columns), the models for  $R_n$  decouple into independent cycle-free factor graphs for every row and every column. For fixed  $\sigma_{\Delta_n}$  (for all  $n$ ) and using (13) and (14), these models for  $R_n$  become linear Gaussian, and their MAP estimates can be computed by forward-backward (or backward-forward) scalar Gaussian message passing.

We thus obtain the following cyclic optimization algorithm for computing the joint MAP estimate of all variables by repeating the following steps until convergence:

- 1) For fixed  $\sigma_{U_n}^2$  and  $R_n = r_n$  (for all  $n$  in all rows and columns), compute the joint MAP estimate of  $U_n, S_n, X_n, Y_n$  by solving the corresponding sparse least-squares problem with the conjugate gradient algorithm.
- 2) For fixed  $U_n = u_n$ , recompute  $\sigma_{U_n}^2$  using (6).
- 3) For fixed  $\sigma_{\Delta_n}^2$ , fixed  $S_n = s_n$ , and using (13) and (14), recompute all  $R_n$  by scalar Gaussian message passing.
- 4) For fixed  $R_n = r_n$ , recompute  $\sigma_{\Delta_n}^2$  by (9).

It is easily seen that the joint MAP estimate of all these variables is a fixed point of this algorithm; beyond that, the algorithm has no guarantees, but empirically works well. Five iterations usually suffice. The computational complexity is dominated by the conjugate gradient algorithm.

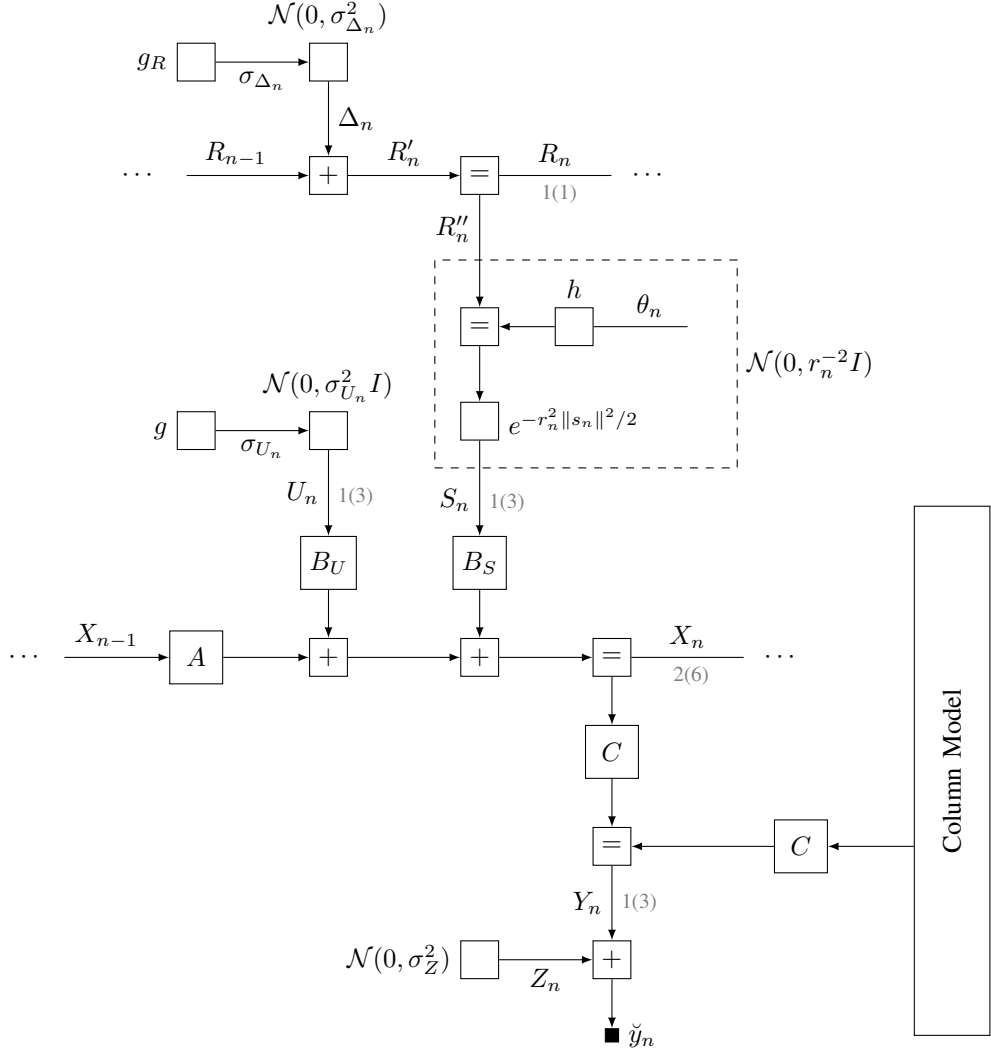


Fig. 1: Factor graph of the basic model, focussing on pixel  $n$  of some row with noisy observation  $\check{Y}_n = \check{y}_n$ . The small gray numbers (e.g., 1(3)) indicate the dimension of the corresponding variables for gray scale and color. The dashed box uses the trick from [10] to reduce the MAP estimation of the slope noise scale factors  $R_n$  to Gaussian message passing.

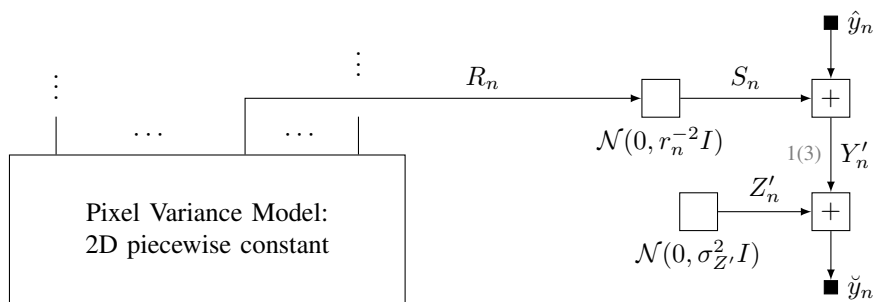


Fig. 2: Factor graph of the augmentation of Section II-D, focussing on a single pixel with noisy observation  $\check{Y}_n = \check{y}_n$ . (The variables  $R_n$  and  $S_n$  are unrelated to the variables with these names in Fig. 1.)

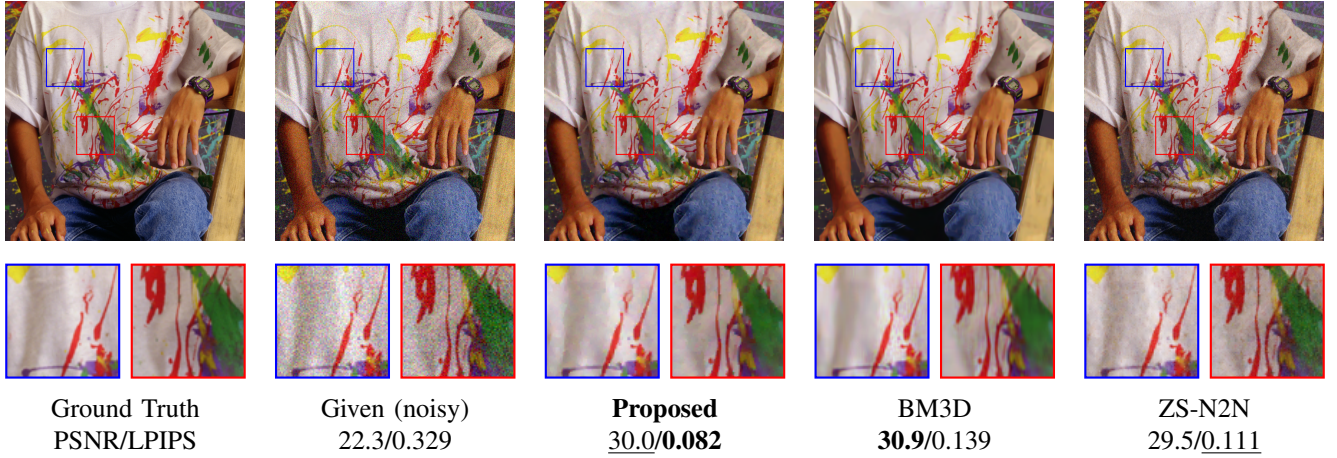


Fig. 3: Example of denoising and comparison with two prior-art methods (BM3D [13], [14] and ZS-N2N [15]). The image is #5 in McMaster18 [16]. The (actual) added Gaussian noise level is  $\sigma = 20/255$ , the assumed parameter  $\sigma_Z$  is  $1/21$ . **Bold** and underline indicate the best and second best scores, respectively. The proposed method produces arguably fewer artifacts.

#### D. Augmented Model and Algorithm

The (optional) augmentation of the model proposed in this section aims at getting back some details (e.g., texture) into the smooth parts that might have been oversmoothed by the basic model. To this end, the latent pixels  $Y_n$  are reinterpreted as a local background, which is estimated with the algorithm of Section II-C. The final estimates of the pixels are obtained by locally adaptive L2 regularization against this background.

Specifically, let  $\hat{y}_n$  be the value of  $Y_n$  that was estimated as described above. The actual pixel value  $Y'_n$  is now modeled as

$$Y'_n = \hat{y}_n + S_n, \quad (15)$$

where  $S_n$  is the deviation<sup>1</sup> from the local background. As in (1), we observe

$$\check{Y}_n = Y'_n + Z'_n, \quad (16)$$

where  $Z'_n$  is white Gaussian noise with fixed variance  $\sigma_{Z'}^2$ , with  $\sigma_{Z'}^2 = \sigma_Z^2$  being a viable choice.

The local deviations  $S_n$  are also modeled as independent zero-mean Gaussian random variables, but with individual variances  $R_n^{-2}$ .

Specifically,  $R_n$  are modeled as (approximately) piecewise constant, as is summarily illustrated in Fig. 2. This is implemented by scalar state space models with sparse increments  $\Delta_n$  as in (7), one such model for each row and each column; these row models and column models are independent, but coupled by the condition that the value of  $R_n$  in the pertinent row model equals its value in the pertinent column model.

The node “ $\mathcal{N}(0, r_n^{-2} I)$ ” in Fig. 2 is implemented like the dashed box in Fig. 1.

We then obtain the following cyclic optimization algorithm for computing the joint MAP estimate of all variables by repeating the following steps until convergence:

<sup>1</sup>In this section, we reuse several variable names (including  $S_n$  and  $R_n$ ) from Sections II-A and II-B for new variables, which facilitates the discussion.

- 1) For fixed  $R_n = r_n$ , compute the (trivial) MAP estimate of  $Y'_n$  for all  $n$ .
- 2) For fixed  $Y'_n = y'_n$ , compute the Gaussian backward message through  $R_n$  using (13) and (14).
- 3) For fixed variances  $\sigma_{\Delta_n}^2$  and fixed backward messages through  $R_n$ , compute the joint MAP estimate of all  $R_n$  using the conjugate gradient algorithm.
- 4) For fixed  $R_n = r_n$ , update the variances  $\sigma_{\Delta_n}^2$  using (9).

As in Section II-C, the joint MAP estimate of all variables is a fixed point of this algorithm, and the computational complexity is dominated by the conjugate gradient algorithm.

### III. APPLICATIONS AND EXPERIMENTS

#### A. Denoising of Gaussian Noise

A first example is shown in Fig. 3. In this example, and in all examples of this subsection, the given noisy image is obtained from a known ground truth by adding i.i.d. Gaussian noise. The numerical scores are the standard peak signal-to-noise ratio (PSNR) and the perceptual loss (LPIPS) from [19].

The effect of the user-defined parameter  $\sigma_Z^2$  is demonstrated in Fig. 4. The effect of the augmented model (vs. the basic model) is demonstrated in Fig. 5.

Table I gives a systematic comparison with several prior-art methods that do not need to be trained on datasets. Note that BM3D and ZS-N2N use nonlocal information within the image and are prone to produce nonlocal artifacts. In these experiments, the parameter  $\sigma_Z$  of the proposed method was adapted to the noise level, but not to individual images.

#### B. Contrast Enhancement

Denoising and contrast enhancement are commonly considered as entirely different tasks requiring entirely different methods. However, the proposed model can easily be used for contrast enhancement as follows. First, the algorithm of Section II-C is used to compute estimates  $\hat{u}_n$  of the level steps  $U_n$ . Second, the level steps are fixed to  $U_n = \varphi(\hat{u}_n)$ , and all

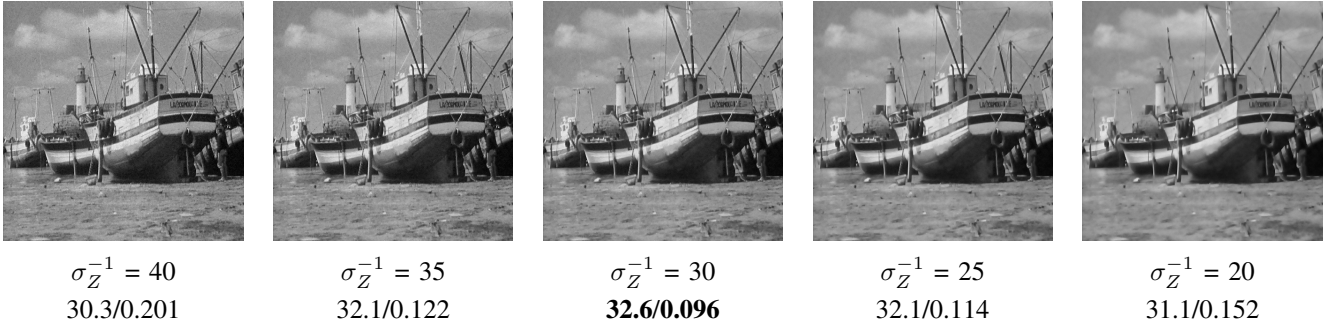


Fig. 4: Effect of the parameter  $\sigma_Z$ , with best numerical scores (PSNR and LPIPS) in **bold**. The image is Boat in [13], the (actual) Gaussian noise level is  $\sigma = 10/255$ .

| Local              | McMaster18 (color) |              |                   |              | Set12 (grayscale) |              |                   |              |
|--------------------|--------------------|--------------|-------------------|--------------|-------------------|--------------|-------------------|--------------|
|                    | $\sigma = 10/255$  |              | $\sigma = 20/255$ |              | $\sigma = 10/255$ |              | $\sigma = 20/255$ |              |
|                    | PSNR               | LPIPS        | PSNR              | LPIPS        | PSNR              | LPIPS        | PSNR              | LPIPS        |
| Noisy image        | 28.5               | 0.149        | 22.7              | 0.365        | 28.1              | 0.251        | 22.2              | 0.513        |
| ✓ TV [1], [2]      | 32.8               | 0.092        | 29.4              | 0.165        | 31.8              | 0.105        | 28.8              | 0.172        |
| ✓ SNUV [8]         | 33.0               | <u>0.049</u> | 29.9              | <u>0.116</u> | 32.4              | <u>0.080</u> | 28.8              | 0.171        |
| ✓ Proposed (augm.) | 33.4               | <b>0.043</b> | 30.4              | <b>0.114</b> | 32.7              | <b>0.075</b> | 29.2              | 0.158        |
| ✓ Proposed (basic) | <u>34.1</u>        | 0.052        | <u>30.6</u>       | 0.123        | 32.6              | 0.096        | 29.1              | 0.181        |
| – BM3D [13], [14]  | <b>35.0</b>        | 0.072        | <b>31.3</b>       | 0.144        | <b>33.7</b>       | 0.084        | <b>30.6</b>       | <b>0.143</b> |
| – ZS-N2N [15]      | 34.1               | 0.054        | 30.2              | 0.122        | 32.3              | 0.082        | 28.5              | 0.182        |

TABLE I: Denoising with the proposed method (with and without the augmentation of Section II-D) and several prior-art methods. The table shows the average numerical scores for data sets McMaster18 [16] and Set12 [17], [18], for two different levels of added Gaussian noise. **Bold** and underline indicate the best and second best scores, respectively.

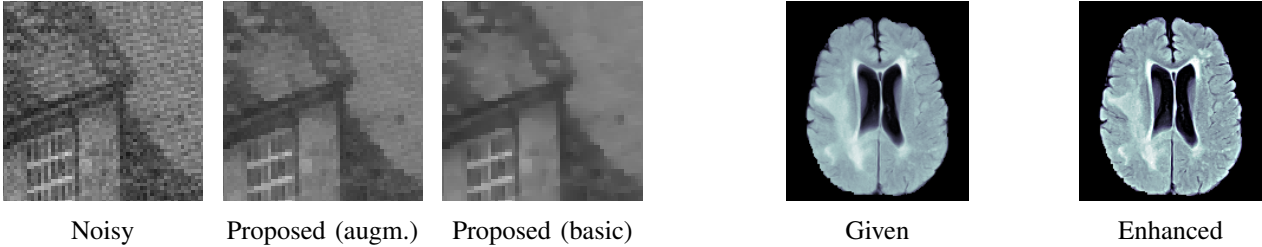


Fig. 5: Denoising with basic model and augmented model. The image is Hill (cropped) from [13] with (actual) Gaussian noise level  $\sigma = 10/255$ .

other variables are restimated. The function  $\varphi(u_n)$  should be symmetric, concave for  $u_n \geq 0$ , and have slope  $> 1$  at  $u_n = 0$ ; e.g.,  $\varphi(u_n) = \alpha \tanh(\beta u_n)$  with  $\beta > 1$ . An exemplary result with this method is shown in Fig. 6. The image in Fig. 6 is a slice of brain MRI scan from BraTS 2018 [20]–[22].

### C. More Applications and Details

More details, applications (including inpainting and non-Gaussian denoising), and examples are given in the appendix of the arXiv version (arXiv:2601.08749).

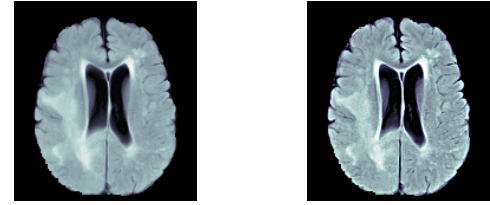


Fig. 6: Example of contrast enhancement.

## IV. CONCLUSION

We proposed a novel image model that is more flexible than prior explicit image models and needs only one (interpretable) parameter to be set by the user. The empirical performance for denoising is arguably at least as good as two specialized prior-art methods. Moreover, the model and algorithms are easily adapted to other tasks including (but not limited to) contrast enhancement, non-Gaussian denoising, and inpainting.

Technically, and of independent interest, the paper exemplifies model-based signal processing in the spirit of [23] with recent advances as summarized in [10].

## V. APPENDIX

### A. Parameter Setting

The default initializations for basic model are  $\sigma_{U_n} = 1/10$ ,  $r_n = 500$ ,  $\sigma_{\Delta_n} = 10$  for all  $n$ . And the default initializations for augmented model are  $\sigma_{Z'} = \sigma_Z$ ,  $r_n = 60$ ,  $\sigma_{\Delta_n} = 10$  for all  $n$ . For both basic and augmented model, five iterations usually suffice.

### B. Basic Model and Augmented Model

The difference between basic model and augmented model is demonstrated in Fig. 7. The bricks in the reconstruction result of augmented model is much more obvious, indicating that the augmented model indeed adds some details back when compared to the basic model.

### C. Effect of Parameter $\sigma_Z^2$

The effect of the user-defined parameter  $\sigma_Z^2$  is demonstrated in other color image examples in Fig. 8. With the increase of  $\sigma_Z^2$ , the denoised images are getting smoother. It is noted that the best scores in BM3D and LPIPS may not be achieved by the same parameter  $\sigma_Z^2$ .

### D. Poissonian-Gaussian Noise

In the case of Poissonian-Gaussian noise, the observation  $\check{Y}_n$  is considered to be obtained by first applying Poisson corruption to pixel  $X_n$  with peak intensity  $\alpha$  (related to the gain of camera) and then adding white Gaussian noise with variance  $\sigma_Z^2$ . Then we have

$$\check{Y}_n = \alpha^{-1} \mathcal{P}(\alpha X_n) + \mathcal{N}(0, \sigma_Z^2). \quad (17)$$

With the common approximation of Poisson noise as the Gaussian noise with equal mean and variance [24], we get

$$\check{Y}_n \approx \alpha^{-1} \mathcal{N}(\alpha X_n, \alpha X_n) + \mathcal{N}(0, \sigma_Z^2). \quad (18)$$

Then the noisy pixel  $\check{Y}_n$  can be regarded as the original pixel  $X_n$  with an additive white Gaussian noise whose variance is relative to the pixel intensity,

$$\check{Y}_n \approx X_n + \mathcal{N}(0, \alpha^{-1} X_n + \sigma_Z^2). \quad (19)$$

Therefore we introduce a new user-defined parameter  $\alpha$  to model the Poissonian-Gaussian noise.

The examples of denoising with Poissonian-Gaussian noise are demonstrated in Figure 8-10. The actual Gaussian noise level is  $\sigma = 10/255$  and actual Poissonian noise peak intensity is 100. The assumed parameter  $\sigma_Z$  is 1/35 and  $\alpha$  is 275.

### E. Contrast Enhancement

As discussed in Section III-B, the function  $\varphi(u_n)$  should be symmetric, concave for  $u_n \geq 0$ , and have slope  $> 1$  at  $u_n = 0$ . There are several choices of function  $\varphi$ , like hyperbolic tangent function,  $\varphi(u_n) = \alpha \tanh(\beta u_n)$  with  $\beta > 1$ . Here we choose another function that is modified with gamma correction as follows:

$$\varphi(u_n) = \begin{cases} \text{sgn}(u_n) \lambda^{\gamma-1} |u_n|, & |u_n| < \lambda, \\ \text{sgn}(u_n) |u_n|^\gamma, & |u_n| \geq \lambda. \end{cases} \quad (20)$$

The contrast enhancement and edge detection are shown in Fig. 12. Here we choose  $\lambda = 0.5$  and  $\gamma = 0.7, 0.5, 0.3$  to elaborate different contrast enhancement effects.

### F. Inpainting

The model can easily adapted to inpainting problem by simply setting the parameter  $\sigma_Z^2$  to be large enough (e.g.  $\sigma_Z^2 = 100$ ) for the area (pixels) that need to be inpainted. Fig. 13 shows the inpainted results of image with words (2-3 pixels width) and random white scratches (1-2 pixels width).

### G. Pseudocode of the Algorithm (steps 2-4) in Section II-C

Forward-backward message passing [23], [25] for one row or one column

**Input:**  $\overleftarrow{W}_{R''_n}, \overleftarrow{\xi}_{R''_n}$  for  $n = 2, 3, \dots, N$

**Output:**  $r_n$  for  $n = 2, 3, \dots, N$ ,  $\sigma_{\Delta_n}^2$  for  $n = 3, 4, \dots, N$

```

1: Forward recursion:
2: Initialize:  $\vec{V}_{R_2} \leftarrow \overleftarrow{W}_{R'_2}^{-1}, \vec{m}_{R_2} \leftarrow \overleftarrow{W}_{R'_2}^{-1} \overleftarrow{\xi}_{R''_2}$ 
3: for  $n = 2, 3, \dots, N-1$  do
4:    $\vec{V}_{R'_{n+1}} \leftarrow \vec{V}_{R_n} + \sigma_{\Delta_{n+1}}^2$ 
5:    $\vec{m}_{R'_{n+1}} \leftarrow \vec{m}_{R_n}$ 
6:    $\vec{W}_{R_{n+1}} \leftarrow \vec{V}_{R'_{n+1}}^{-1} + \overleftarrow{W}_{R''_{n+1}}$ 
7:    $\overleftarrow{\xi}_{R_{n+1}} \leftarrow \vec{V}_{R'_{n+1}}^{-1} \vec{m}_{R'_{n+1}} + \overleftarrow{\xi}_{R''_{n+1}}$ 
8:    $\vec{V}_{R_{n+1}} \leftarrow \vec{W}_{R_{n+1}}^{-1}$ 
9:    $\vec{m}_{R_{n+1}} \leftarrow \vec{W}_{R_{n+1}}^{-1} \overleftarrow{\xi}_{R_{n+1}}$ 
10: end for
11: Backward recursion:
12: Initialize:  $\overleftarrow{W}_{R_N} \leftarrow 0, \overleftarrow{\xi}_{R_N} \leftarrow 0$ 
13: for  $n = N, N-1, \dots, 3$  do
14:    $\overleftarrow{W}_{R'_n} \leftarrow \overleftarrow{W}_{R_n} + \overleftarrow{W}_{R''_n}$ 
15:    $\overleftarrow{\xi}_{R'_n} \leftarrow \overleftarrow{\xi}_{R_n} + \overleftarrow{\xi}_{R''_n}$ 
16:    $\overleftarrow{V}_{R_{n-1}} \leftarrow \overleftarrow{W}_{R'_n}^{-1} + \sigma_{\Delta_n}^2$ 
17:    $\overleftarrow{m}_{R_{n-1}} \leftarrow \overleftarrow{W}_{R'_n}^{-1} \overleftarrow{\xi}_{R'_n}$ 
18:    $\overleftarrow{W}_{R_{n-1}} = \overleftarrow{V}_{R_{n-1}}^{-1}$ 
19:    $\overleftarrow{\xi}_{R_{n-1}} = \overleftarrow{W}_{R_{n-1}} \overleftarrow{m}_{R_{n-1}}$ 
20: end for
21: Compute posterior mean:
22: for  $n = 2, 3, \dots, N$  do
23:    $r_n \leftarrow \frac{\vec{V}_{R_n}^{-1} \vec{m}_{R_n} + \overleftarrow{V}_{R_n}^{-1} \overleftarrow{m}_{R_n}}{\vec{V}_{R_n}^{-1} + \overleftarrow{V}_{R_n}^{-1}}$ 
24: end for
25: Update NUP parameters ( $\theta_n$  is updated implicitly [10]):
26: for  $n = 3, 4, \dots, N$  do
27:    $\Delta_n \leftarrow r_n - r_{n-1}$ 
28:    $\sigma_{\Delta_n}^2 \leftarrow \frac{\|\Delta_n\|^{2-p}}{\beta_{\Delta p}}$ 
29: end for

```

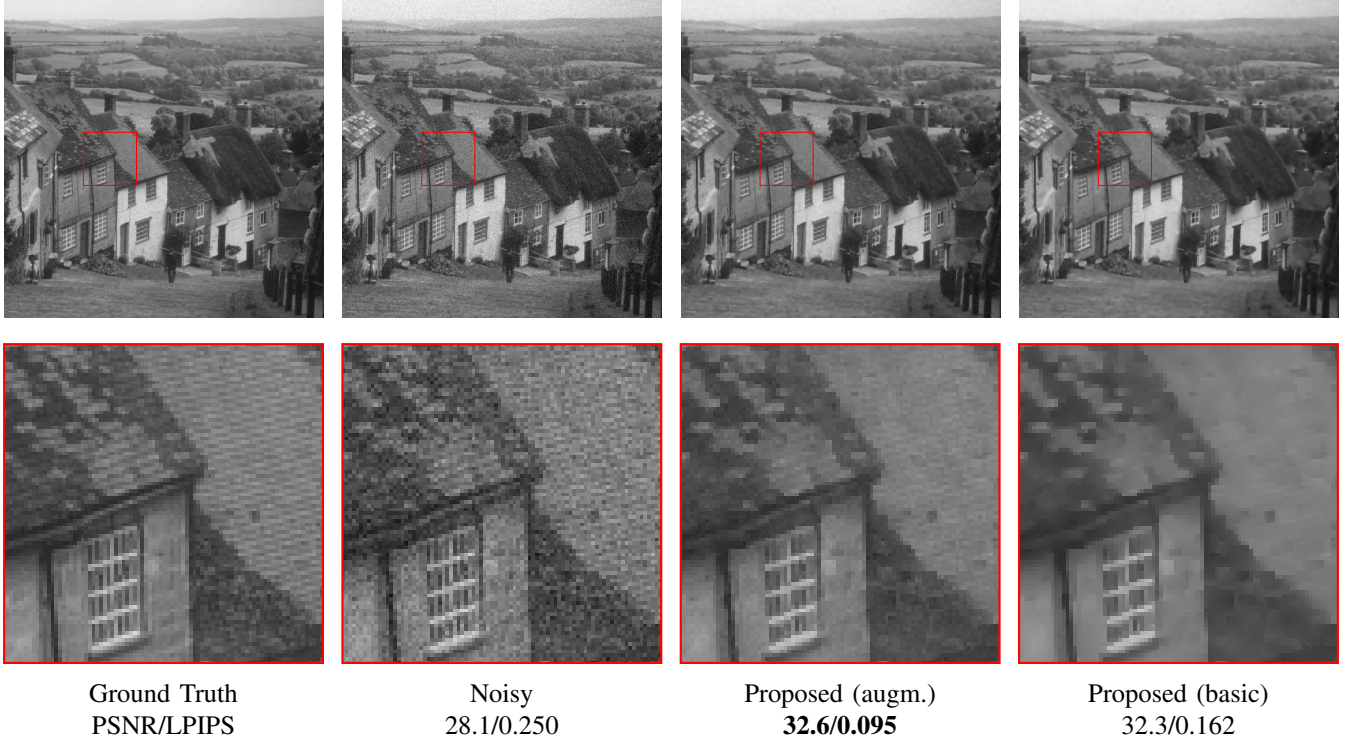


Fig. 7: Visual comparison of image Hill in [13] for Gaussian noise level  $\sigma = 10/255$ . The quantitative PSNR/LPIPS results are given below the image. **Bold** indicates the best results.

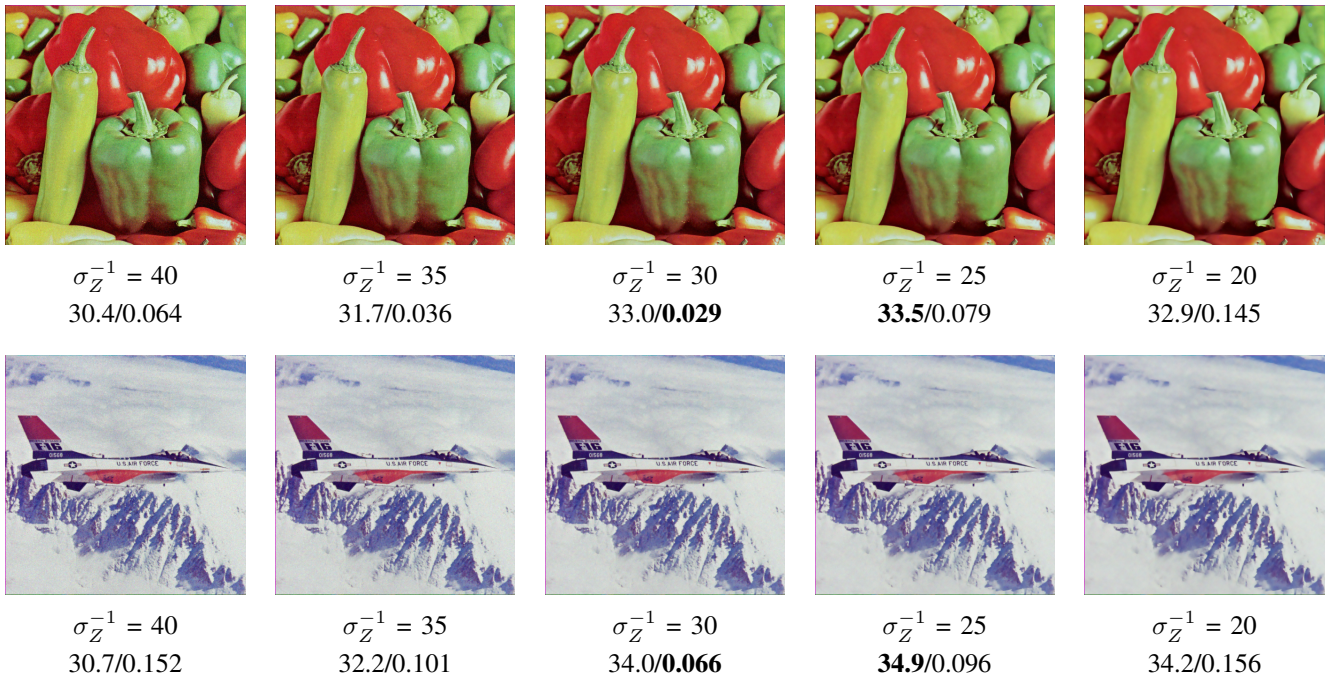


Fig. 8: Effect of the parameter  $\sigma_Z$ , with best numerical scores (PSNR/LPIPS) in **bold**. The images are Peppers and F16 in [13], the (actual) Gaussian noise level is  $\sigma = 10/255$ .

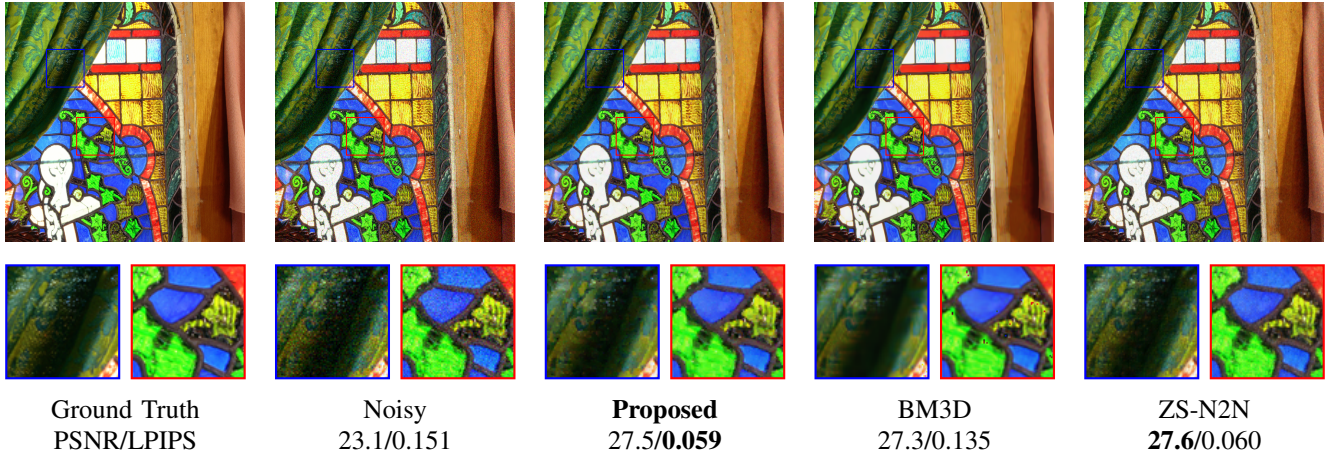


Fig. 9: Visual comparison of image #1 in McMaster18 [16] for Gaussian noise level  $\sigma = 10/255$  and Poissonian noise with peak intensity 100. **Bold** and underline indicate the best and second best results, respectively.

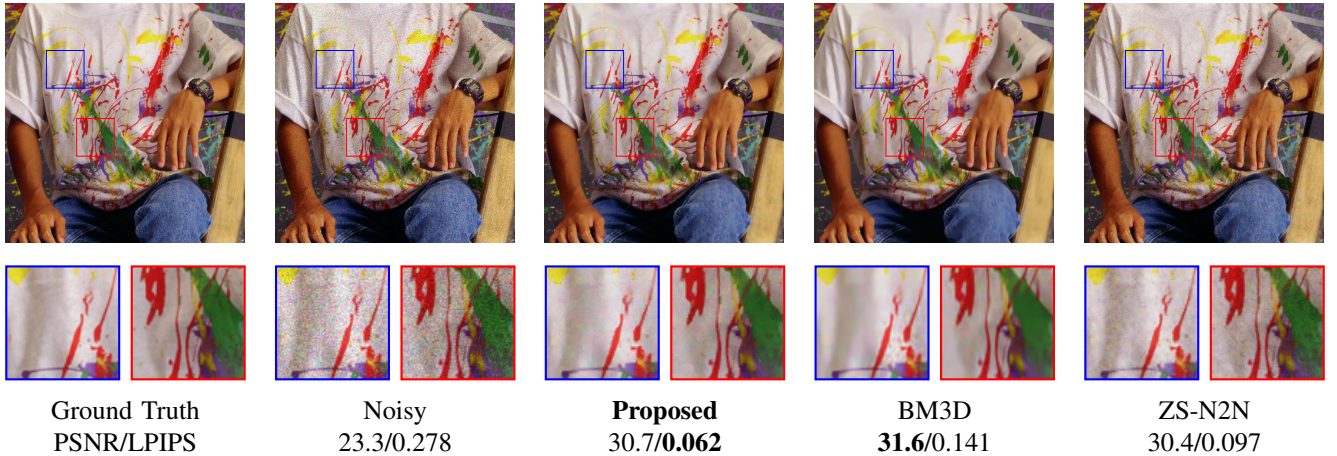


Fig. 10: Visual comparison of image #5 in McMaster18 [16] for Gaussian noise level  $\sigma = 20/255$  and Poissonian noise with peak intensity 100. **Bold** and underline indicate the best and second best results, respectively.



Fig. 11: Visual comparison of image #10 in McMaster18 [16] for Gaussian noise level  $\sigma = 20/255$  and Poissonian noise with peak intensity 100. **Bold** and underline indicate the best and second best results, respectively.

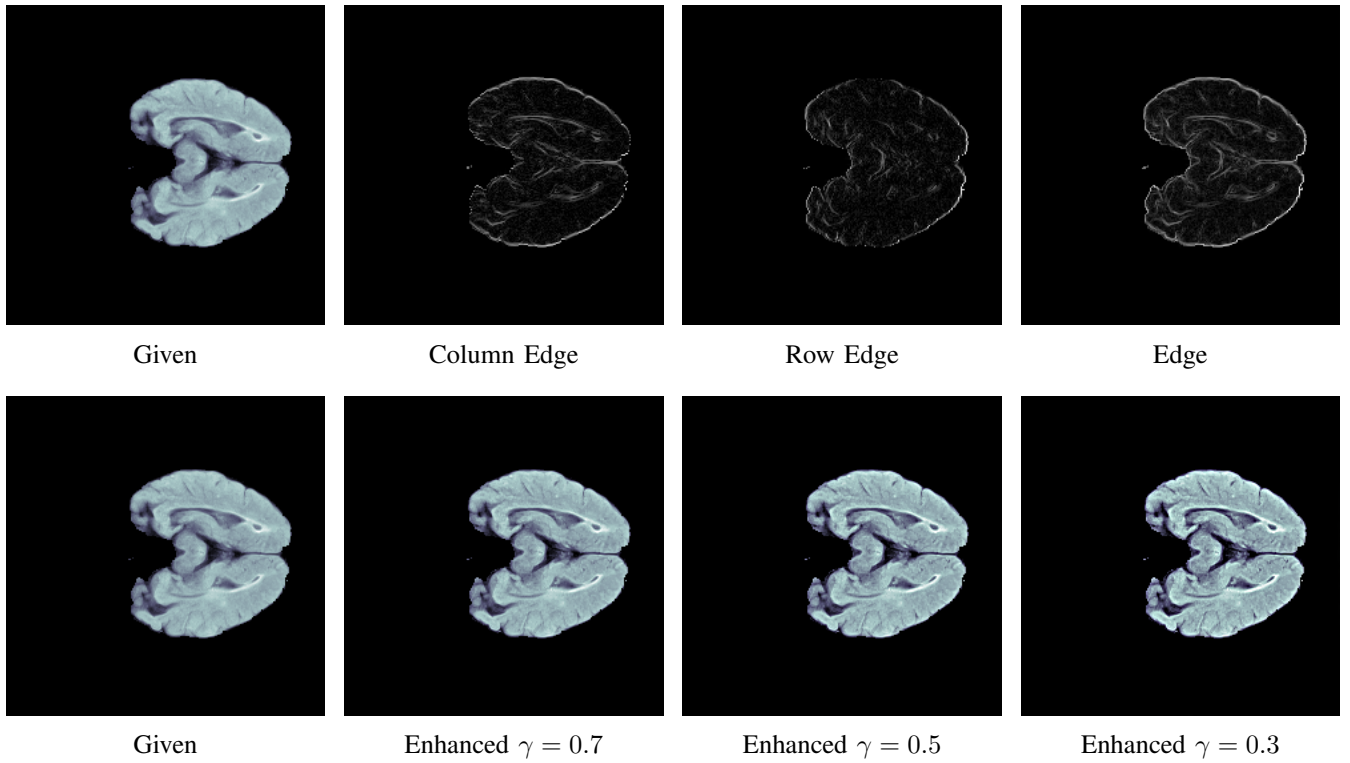


Fig. 12: Experiments of local contrast enhancement. The image is a slice of brain MRI scan from BraTS 2018 [20]–[22].

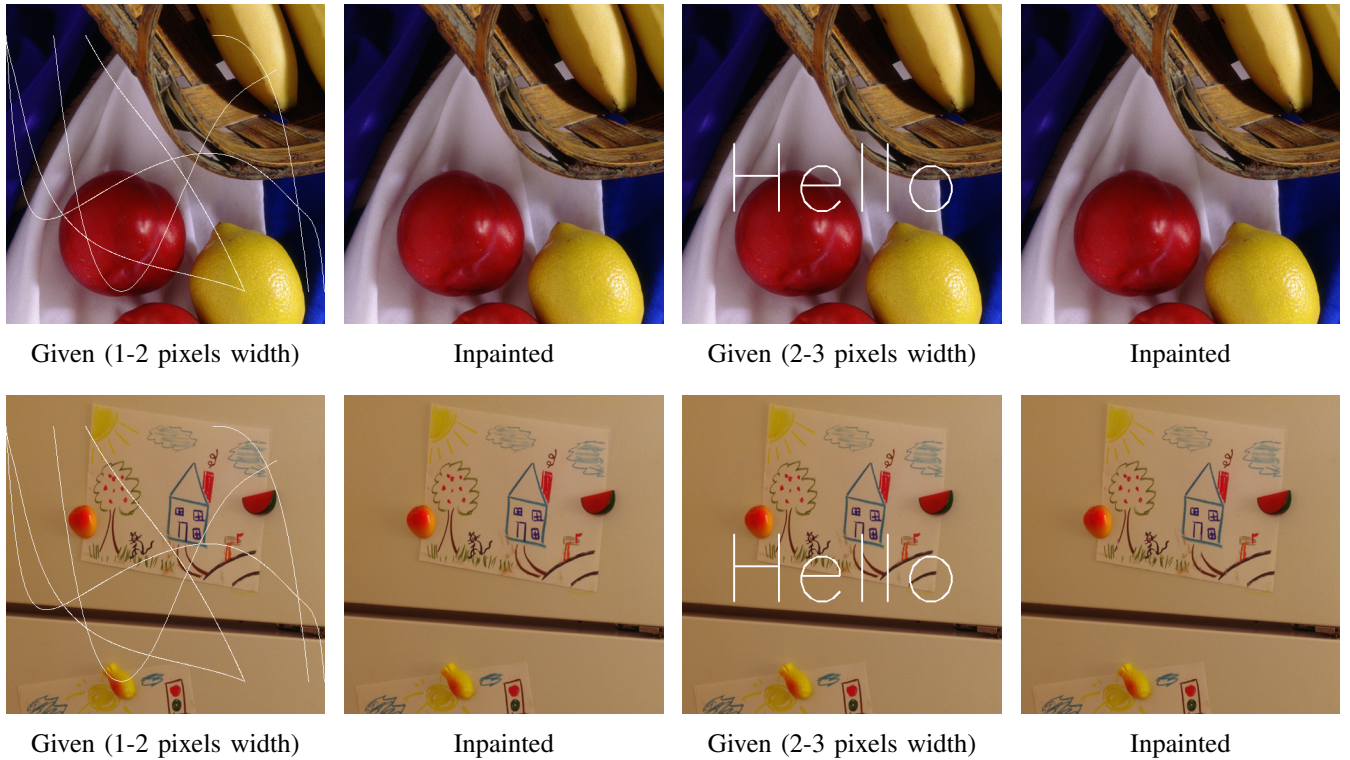


Fig. 13: Experiments of image inpainting. The images are #13 and #14 in McMaster18 [16].

## REFERENCES

- [1] L. I. Rudin, S. Osher, and E. Fatemi, “Nonlinear total variation based noise removal algorithms,” *Physica D: Nonlinear Phenomena*, vol. 60, no. 1-4, pp. 259–268, 1992.
- [2] A. Chambolle, “An algorithm for total variation minimization and applications,” *Journal of Mathematical Imaging and Vision*, vol. 20, pp. 89–97, 2004.
- [3] K. Bredies, K. Kunisch, and T. Pock, “Total generalized variation,” *SIAM Journal on Imaging Sciences*, vol. 3, no. 3, pp. 492–526, 2010.
- [4] S. Lefkimmiatis, A. Roussos, P. Maragos, and M. Unser, “Structure tensor total variation,” *SIAM Journal on Imaging Sciences*, vol. 8, no. 2, pp. 1090–1122, 2015.
- [5] A. Yezzi, “Modified curvature motion for image smoothing and enhancement,” *IEEE Transactions on Image Processing*, vol. 7, no. 3, pp. 345–352, 1998.
- [6] W. Zhu and T. Chan, “Image denoising using mean curvature of image surface,” *SIAM Journal on Imaging Sciences*, vol. 5, no. 1, pp. 1–32, 2012.
- [7] Q. Zhong, Y. Li, Y. Yang, and Y. Duan, “Minimizing discrete total curvature for image processing,” in *Proceedings of the IEEE/CVF Conference on Computer Vision and Pattern Recognition*, 2020, pp. 9474–9482.
- [8] B. Ma, N. Zalmai, and H.-A. Loeliger, “Smoothed-NUV priors for imaging,” *IEEE Transactions on Image Processing*, vol. 31, pp. 4663–4678, 2022.
- [9] H.-A. Loeliger, B. Ma, H. Malmberg, and F. Wadehn, “Factor graphs with NUV priors and iteratively reweighted descent for sparse least squares and more,” 10th International Symposium on Turbo Codes & Iterative Information Processing (ISTC), 2018.
- [10] H.-A. Loeliger, “On NUP priors and Gaussian message passing,” IEEE 33rd International Workshop on Machine Learning for Signal Processing (MLSP), Rome, Italy, 2023.
- [11] F. Bach, R. Jenatton, J. Mairal, G. Obozinski *et al.*, “Optimization with sparsity-inducing penalties,” *Foundations and Trends in Machine Learning*, vol. 4, no. 1, pp. 1–106, 2012.
- [12] A. Lukaj and H.-A. Loeliger, “Automatic regularization and multiple scale factor estimation in linear Gaussian and non-Gaussian models,” submitted to ISIT 2026.
- [13] K. Dabov, A. Foi, V. Katkovnik, and K. Egiazarian, “Image denoising with block-matching and 3d filtering,” in *Image Processing: Algorithms and Systems, Neural Networks, and Machine Learning*, vol. 6064, 2006, pp. 354–365.
- [14] K. Dabov, A. Foi, V. Katkovnik, and K. Egiazarian, “Image denoising by sparse 3-D transform-domain collaborative filtering,” *IEEE Transactions on Image Processing*, vol. 16, no. 8, pp. 2080–2095, 2007.
- [15] Y. Mansour and R. Heckel, “Zero-Shot Noise2Noise: Efficient image denoising without any data,” in *Proceedings of the IEEE/CVF Conference on Computer Vision and Pattern Recognition*, 2023, pp. 14 018–14 027.
- [16] L. Zhang, X. Wu, A. Buades, and X. Li, “Color demosaicking by local directional interpolation and nonlocal adaptive thresholding,” *Journal of Electronic Imaging*, vol. 20, no. 2, pp. 023 016–023 016, 2011.
- [17] K. Zhang, W. Zuo, Y. Chen, D. Meng, and L. Zhang, “Beyond a Gaussian denoiser: Residual learning of deep CNN for image denoising,” *IEEE Transactions on Image Processing*, vol. 26, no. 7, pp. 3142–3155, 2017.
- [18] K. Zhang, W. Zuo, and L. Zhang, “FFDNet: Toward a fast and flexible solution for CNN-based image denoising,” *IEEE Transactions on Image Processing*, vol. 27, no. 9, pp. 4608–4622, 2018.
- [19] R. Zhang, P. Isola, A. A. Efros, E. Shechtman, and O. Wang, “The unreasonable effectiveness of deep features as a perceptual metric,” in *Proceedings of the IEEE Conference on Computer Vision and Pattern Recognition*, 2018, pp. 586–595.
- [20] B. H. Menze, A. Jakab, S. Bauer, J. Kalpathy-Cramer, K. Farahani, J. Kirby, Y. Burren, N. Porz, J. Slotboom, R. Wiest *et al.*, “The multimodal brain tumor image segmentation benchmark (BRATS),” *IEEE Transactions on Medical Imaging*, vol. 34, no. 10, pp. 1993–2024, 2014.
- [21] S. Bakas, H. Akbari, A. Sotiras, M. Bilello, M. Rozycski, J. S. Kirby, J. B. Freymann, K. Farahani, and C. Davatzikos, “Advancing the cancer genome atlas glioma MRI collections with expert segmentation labels and radiomic features,” *Scientific Data*, vol. 4, no. 1, pp. 1–13, 2017.
- [22] S. Bakas, M. Reyes, A. Jakab, S. Bauer, M. Rempfler, A. Crimi, R. T. Shinohara, C. Berger, S. M. Ha, M. Rozycski *et al.*, “Identifying the best machine learning algorithms for brain tumor segmentation, progression assessment, and overall survival prediction in the BRATS challenge,” *arXiv preprint arXiv:1811.02629*, 2018.
- [23] H.-A. Loeliger, J. Dauwels, J. Hu, S. Korl, L. Ping, and F. R. Kschischang, “The factor graph approach to model-based signal processing,” *Proceedings of the IEEE*, vol. 95, no. 6, pp. 1295–1322, 2007.
- [24] A. Foi, M. Trimeche, V. Katkovnik, and K. Egiazarian, “Practical Poissonian-Gaussian noise modeling and fitting for single-image raw-data,” *IEEE Transactions on Image Processing*, vol. 17, no. 10, pp. 1737–1754, 2008.
- [25] H.-A. Loeliger, L. Bruderer, H. Malmberg, F. Wadehn, and N. Zalmai, “On sparsity by NUV-EM, Gaussian message passing, and Kalman smoothing,” *Information Theory and Applications Workshop (ITA)*, San Diego, CA, 2016.